

## B content and Si/C ratios from cultured diatoms (*Thalassiosira pseudonana* and *Thalassiosira weissflogii*): Relationship to seawater pH and diatom carbon acquisition

Luz María Mejía<sup>a,\*</sup>, Kirsten Isensee<sup>b</sup>, Ana Méndez-Vicente<sup>a</sup>, Jorge Pisonero<sup>c</sup>, Nobumichi Shimizu<sup>d</sup>, Cristina González<sup>c</sup>, Brian Monteleone<sup>d</sup>, Heather Stoll<sup>a</sup>

<sup>a</sup> Dept. Geología, Universidad de Oviedo, Arias de Velasco s/n, 33005 Oviedo, Asturias, Spain

<sup>b</sup> Dept. Biología de Organismos y Sistemas, Universidad de Oviedo, Catedrático Rodrigo Uria s/n, 33006 Oviedo, Asturias, Spain

<sup>c</sup> Dept. Física, Universidad de Oviedo, Calvo Sotelo s/n, 33005 Oviedo, Asturias, Spain

<sup>d</sup> Geology and Geophysics Dept., Woods Hole Oceanographic Institute, Woods Hole, MA, USA

Received 27 July 2012; accepted in revised form 6 June 2013; available online 18 June 2013

### Abstract

Despite the importance of diatoms in regulating climate and the existence of large opal-containing sediments in key air-ocean exchange areas, most geochemical proxy records are based on carbonates. Among them, Boron (B) content and isotopic composition have been widely used to reconstruct pH from foraminifera and coral fossils. We assessed the possibility of a pH/CO<sub>2</sub> seawater concentration control on B content in diatom opal to determine whether or not frustule B concentrations could be used as a pH proxy or to clarify algae physiological responses to acidifying pH. We cultured two well-studied diatom species, *Thalassiosira pseudonana* and *Thalassiosira weissflogii* at varying pH conditions and determined Si and C quotas. Frustule B content was measured by both laser-ablation inductively coupled mass spectrometry (LA-ICPMS) and secondary ion mass spectrometry (SIMS/ion probe). For both species, frustules grown at higher pH have higher B contents and higher Si requirements per fixed C. If this trend is representative of diatom silicification in a future more acidic ocean, it could contribute to changes in the efficiency of diatom ballasting and C export, as well as changes in the contribution of diatoms relative to other phytoplankton groups in Si-limited regions. If B enters the cell through the same transporter employed for HCO<sub>3</sub><sup>-</sup> uptake, an increased HCO<sub>3</sub><sup>-</sup> requirement with decreasing CO<sub>2</sub> concentrations (higher pH), and higher B(OH)<sub>4</sub><sup>-</sup>/HCO<sub>3</sub><sup>-</sup> ratios would explain the observed increase in frustule B content with increasing pH. The mechanism of B transport from the site of uptake to the site of silica deposition is unknown, but may occur via silicon transport vesicles, in which B(OH)<sub>4</sub><sup>-</sup> may be imported for B detoxification and/or as part of a pH regulation strategy either through Na-dependent B(OH)<sub>4</sub><sup>-</sup>/Cl<sup>-</sup> antiport or B(OH)<sub>4</sub><sup>-</sup>/H<sup>+</sup> antiport. B deposition in the silica matrix may occur via substitution of a B(OH)<sub>4</sub><sup>-</sup> for a negatively charged SiO<sup>-</sup> formed during silicification. With the current analytical precision, B content of frustules is unlikely to resolve ocean pH with a precision of paleoceanographic interest. However, if frustule B content was controlled mainly by HCO<sub>3</sub><sup>-</sup> uptake for

*Abbreviations:* SDV, silicon deposition vesicle; STV, silicon transport vesicle; LA-ICPMS, laser-ablation inductively coupled mass spectrometry; SIMS/Ion probe, secondary ion mass spectrometry; CCM, carbon concentration mechanisms; CCF, carbon concentration factor

\* Corresponding author. Tel.: +34 691 957 244.

E-mail address: [luzmamera2@yahoo.com](mailto:luzmamera2@yahoo.com) (L.M. Mejía).

photosynthesis, which appears to show a threshold behavior, then measurements of B content might reveal the varying importance of active  $\text{HCO}_3^-$  acquisition mechanisms of diatoms in the past.

© 2013 The Authors. Published by Elsevier Ltd. Open access under [CC BY-NC-ND license](#).

## 1. INTRODUCTION

Diatoms are very important climate modulators because they account for 40% of marine primary production (Nelson et al., 1995) and are responsible for more than 50% of the export of carbon from the photic zone (Dugdale and Wilkerson, 1998). Consequently, they are key regulators of atmospheric  $\text{CO}_2$  concentrations worldwide, especially in nutrient-rich regions such as the Southern Ocean and upwelling areas. Diatoms dominate the phytoplankton community wherever and whenever conditions are optimal for phytoplankton growth (Ragueneau et al., 2000), being the world's largest contributors to biosilicification (Martin-Jézéquel et al., 2000). Ballasting of sinking organic aggregates containing diatom frustules, while potentially less efficient than ballasting by coccoliths (Iversen and Ploug, 2010), increases the sinking velocity of particles by several-fold (Ploug et al., 2008). Nonetheless, while the response of coccolith biomineralization to changing seawater carbonate chemistry has been widely explored in the past decade (Riebesell et al., 2000; Langer et al., 2006, 2009), the response of opal silica production has received much more limited attention (Milligan et al., 2004). If opal production serves as a pH buffer for enzymes used for carbon acquisition by diatoms (Milligan and Morel, 2002) then opal production and Si/C may also be sensitive to changes in the relative availability of the main carbon sources ( $\text{CO}_2$  and  $\text{HCO}_3^-$ ) in the future ocean. Whereas previous studies have reported the cellular Si quota, here we present in addition the Si/C ratio which controls for any variation in cell size which affects both C and Si quotas, and provides the key parameter for understanding marine biogeochemical cycles, the ratio of Si required for each mole of C fixed.

There are diatom-bearing sediments in key regions of air-sea  $\text{CO}_2$  exchange like the Southern Ocean, in which traditional carbonate sources of geochemical proxy records (e.g. foraminifera) are scarce or absent. This suggests that diatoms may also be an important phase for geochemical proxies. One key proxy widely used to explore changes in the ocean carbon chemistry, is the boron (B) content and isotopic composition of marine biominerals. Boron speciation in seawater is pH dependent, with boric acid ( $\text{B}(\text{OH})_3$ ) dominant below pH  $\sim 8.85$  and borate ( $\text{B}(\text{OH})_4^-$ ) dominant at pH  $> \sim 8.85$  (NBS scale) (Fig. 1). Both in biogenic carbonates (aragonite and calcite) and inorganic carbonates, the substitution of  $\text{B}(\text{OH})_4^-$  ion favors higher B content at higher pH (Sanyal et al., 2000; Fietzke et al., 2010). A strong fractionation of  $^{10}\text{B}$  and  $^{11}\text{B}$  between  $\text{B}(\text{OH})_4^-$  and  $\text{B}(\text{OH})_3$  also results in a pH sensitivity to the  $\delta^{11}\text{B}$  in marine carbonates, widely exploited to reconstruct seawater pH from foraminifera (Seki et al., 2010; Bartoli et al., 2011; Rae et al., 2011). However, foraminifera, unlike diatoms, produce biominerals directly from seawater (Bentov et al., 2009), making them more likely to record seawater carbonate

chemistry, although modification of pH in the calcifying vesicle may also influence the reconstruction (Rollion-Bard and Erez, 2010).

Diatom biomineralization, in contrast, is characterized by maintenance of highly acidic pH in the site of biomineralization and occurs far from the pK of the boron speciation. Diatom opal is formed by the condensation and polymerization of silicic acid monomers in a specialized cellular compartment known as the silicon deposition vesicle (SDV) (Martin-Jézéquel et al., 2000). The acidic pH of  $\sim 5$  is tightly regulated inside the SDV in order to promote monomer auto-polymerization (Vrieling et al., 1999), avoid frustule malformations due to acidic-required conditions by biomineralizing proteins (Kröger et al., 2000) and possibly save energy during frustule deposition. If this pH control limits the cellular biological overprint on the opal B content or isotopic composition, diatom opal might complement existing carbonate proxies. If, however, biological transport mechanisms of B into the cell strongly affect the diatom B content and isotopic composition, as suggested recently for coccolithophorid algae (Stoll et al., 2012), then the B system may trace physiological processes in this algal class and reveal more about its role in past and possible future changes in the marine carbon cycle.

Two well studied diatoms species were cultured, *Thalassiosira pseudonana* and *Thalassiosira weissflogii*, at a range of seawater pH and dissolved  $\text{CO}_2$  concentrations, to examine the response of silica production and opal B content to changing seawater carbonate chemistry. We determined the Si quotas and Si/C of cells and measured B content with two analytical approaches, laser-ablation inductively coupled mass spectrometry (LA-ICPMS) and secondary ion mass spectrometry (SIMS/ion probe). The correlation between frustule B content and the degree of cellular  $\text{HCO}_3^-$  uptake suggest that the B content may be closely related to the source of carbon used for photosynthesis and its rate of uptake.

## 2. METHODS

### 2.1. Diatom culturing

Diatoms of species *T. pseudonana* (strain SAG 1020-1b) and *T. weissflogii* (strain CCMP 1010) were grown in sterile and filtered seawater (0.2  $\mu\text{m}$  pore size filters) at a controlled temperature of 18 °C and a 16/8 h light/dark cycle. K/5 media enriched with silicate (Keller et al., 1987) to 100  $\mu\text{mol L}^{-1}$  was used for both species. Cultures were incubated on a rolling system to keep cells and media homogeneous inside the bottles. Pre-adaptation for each experimental condition was performed for at least four cell generations. Seawater pH was regulated by addition of 0.5  $\text{mol L}^{-1}$  NaOH or HCl to the initial media. Cell concentrations were continuously monitored to ensure they

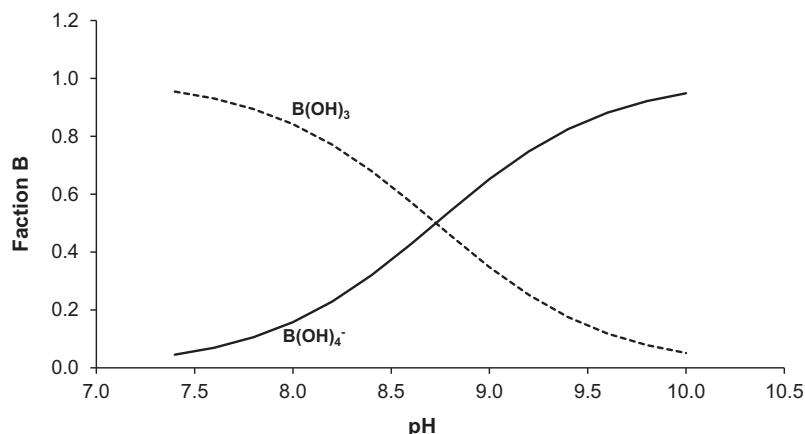


Fig. 1. Fraction of B in seawater present as boric acid ( $\text{B(OH)}_3$ ) and borate ( $\text{B(OH)}_4^-$ ) as a function of pH assuming a salinity of 35 and temperature of 20 °C (Dickson et al., 2007).

remained low enough to avoid significant changes in the carbonate system. *T. pseudonana* and *T. weissflogii* were grown at pH ranges from 7.50 to 8.63 and from 7.54 to 8.33 (NBS scale), respectively. The potential effect of growth rate on B content was assessed as well by varying light intensity using none, one, or two layers of spectrally neutral mesh on cultures of similar pH.

Cell counts, growth rates, total alkalinity (TA) and pH (NBS) were monitored during each experiment following standard procedures similar to those described in (Rost et al., 2006; Trimborn et al., 2009). For some experiments, the source of C for photosynthesis ( $\text{CO}_2/\text{HCO}_3^-$ ) was additionally characterized using the  $^{14}\text{C}$  disequilibrium method (Elzenga et al., 2000; Rost et al., 2007).

Diatoms were collected on 3  $\mu\text{m}$  pore polycarbonate filters and stored in petri dishes. Material used to clean, mount and store diatom opal for B analysis was either acid-cleaned and rinsed with high purity (Milli-Q) de-ionized distilled water or was new and sonicated in Milli-Q to prevent contamination.

## 2.2. Measurement of Si and C quotas

For C quotas, cells were filtered onto precombusted quartz fiber filters and stored frozen at  $-20\text{ }^\circ\text{C}$ . Immediately prior to analysis, cells were dried at  $60\text{ }^\circ\text{C}$  for 2 h and loaded into tin capsules. C yield was measured on a Eurovector Elemental Analyzer (EuroEA3000) connected to Nu Instruments Horizon mass spectrometer at the University of Oviedo. C amounts were quantified from the mass 44 peak area, calibrated with precisely weighed glutamic acid standards.

For measurement of Si quotas, cells were collected on 3  $\mu\text{m}$  pore polycarbonate filters and were stored in 15 mL PP falcon tubes. Filters were dried for at least 12 h at  $60\text{ }^\circ\text{C}$  and cell digestion was achieved using freshly prepared 0.2 N NaOH, heating at  $100\text{ }^\circ\text{C}$  for 40 min and neutralizing using 1 N HCl, following the method described by Ragueneau and Tréguer (1994) and Ragueneau et al. (2005). Si measurements were conducted via ICP-OES (Thermo ICAP 6300 DUO at University of Oviedo).

Complete digestion of cells by NaOH and viability of Si measurements using ICP-OES analysis was tested by filtering different volumes of the same diatom culture and obtaining comparable Si quotas. Relative standard error (r.s.e) of replicates was  $<4\%$ .

## 2.3. Preparation of samples for B content measurement

### 2.3.1. Cleaning frustules of organic matter

Since cultured cells have not been subjected to the long and active process of bacterial oxidation of cellular organic phases, as fossil diatoms have, organic matter content is higher and should be completely oxidized to eliminate possible B contamination present in organic phases outside the biomineral. Harvested cells were detached from filters and frozen in Milli-Q for at least one night to open frustules. Organic matter was oxidized using potassium permanganate and perchloric acid, which was demonstrated to obtain an efficient and total removal of extra-frustule organic matter from cultures, as described by Horn et al. (2011). Samples were dried and stored in Milli-Q sonicated eppendorfs. For a small subset of *T. pseudonana* samples, we examined the impact of cleaning only with the potassium permanganate step and upon ion probe analysis these samples showed more than 30-fold higher  $^{32}\text{S}/^{30}\text{Si}$  ratios ( $6\text{--}7 \times 10^{-3}$ ) compared to the average of fully-cleaned samples ( $1 \times 10^{-4}$ ), suggesting the presence of remaining S-containing organic phases in samples treated with only the first oxidation step. For ICP-MS analysis, small amounts of organics have been shown to produce non-spectrometric effects in the plasma whose result is increasing sensitivity in low mass range (e.g.  $^{11}\text{B}$ ) relative to higher masses (e.g.  $^{29}\text{Si}$ ) and therefore biasing results (Hu et al., 2004). Consequently we report B concentrations only from fully cleaned samples.

### 2.3.2. Mounting cleaned frustules

Sample mounting was carefully performed inside a certified ISO-6 clean-lab fitted with polycarbonate HEPA filters, rather than borosilicate glass filters, to minimize airborne B load. Some samples were mounted on indium, the substrate conventionally used for ion probe analysis, and all samples

were mounted in epoxy, which served both for ion probe and LA-ICPMS analysis.

**2.3.2.1. Indium.** Indium is a soft metal and is conventionally used for ion probe analysis because it is conductive and drains charge effectively. Indium mounts were prepared from 99.9999% pure (metals basis) Indium shot (Alfa Aesar, Puratronic®) in aluminum holders with a hollow central area of ~10 mm diameter and ~4 mm depth. All surfaces in contact with the indium and diatom sample were cleaned by three 5-min cycles of ultrasonication in Milli-Q ultrapure water. A smooth indium surface was ensured by repeated pressing against a polished aluminum disk. The indium disk was prepared to receive samples by indenting areas of ~1 mm diameter with a pipet tip.

Opal frustules were suspended in 50–100 µL Milli-Q. These dense drops were repeatedly deposited on top of the demarcated circle and dried on a hotplate at ~40 °C until a homogeneous white surface covering the whole circle could be observed (Electronic annex EA-1b). Samples were then repressed for 15 min against a cleaned-polished aluminum disk to reduce porosity and topography.

Before ion probe analysis, mounts were placed in the oven and/or vacuum chamber for at least 5 h to eliminate possible water present in samples. They were subsequently gold-coated for 280 s (30 nm gold), repressed and gold coated again to reduce variability of measurements, as found by Stoll et al. (2012).

**2.3.2.2. Epoxy.** Epoxy must be poured over diatoms on a substrate or mold that is clean, smooth, and sufficiently flexible to peel off the cured epoxy and reveal diatoms on the surface. We found that disposable 70 mm aluminum weighing dishes (Fisher Scientific, Madrid, Spain) could be prepared to satisfy these criteria. The basal portion of the dish was polished with diamond grit from Struers (Mol3 DiaPro, Rotherham, UK), then sonicated in acetone to remove any waxes present from manufacture, and sonicated subsequently in Milli-Q. Suspended opal, prepared as in the previous section, was deposited by dropping–drying (0–30 °C) on the polished–cleaned aluminum weighting dishes until a homogeneous white surface was obtained (Electronic annex EA-1a). A cleaned aluminum 10–21 mm ring was placed around the deposited samples and was carefully filled with Struers epoxy (Rotherham, UK). After the resin was dry (at least 12 h), mounts were peeled off the aluminum disk and stored in cleaned plastic boxes (Electronic annex EA-1c).

## 2.4. B/Si analysis

### 2.4.1. Ion probe

Indium (*T. pseudonana*) and epoxy (*T. weissflogii*)-mounted samples were measured on the Cameca IMS 1280 at the Woods Hole Oceanographic Institution using a primary beam of  $^{16}\text{O}^-$  ions and a mass resolution of 2000. We measured  $^{30}\text{Si}$  and  $^{11}\text{B}$ , with a low primary beam current (1–3.5 nA) to prevent  $^{30}\text{Si}$  saturation of the electron multiplier.  $^{32}\text{S}$  was measured on a subset of samples as an indicator of possible organic matter contamination when only permanganate oxidation was used. We applied

counting times of 10, 3 and 2 s for  $^{11}\text{B}$ ,  $^{30}\text{Si}$  and  $^{32}\text{S}$ , respectively and waiting times of 2–3 s. Efforts to measure  $^{10}\text{B}$  were abandoned as there was highly variable  $^{10}\text{B}/^{11}\text{B}$  instrumental fractionation during frustule and standard sputtering possibly due to surface charging or surface topography effects.  $^{11}\text{B}$  count rates were between  $1.3 \times 10^2$  and  $1.5 \times 10^3$  counts per second (cps), while  $^{30}\text{Si}$  count rates remained between  $2.3 \times 10^5$  and  $1.7 \times 10^6$  cps. A raster of 50 µm diameter and a field aperture size of 2002 were used, so that a central area of  $38 \times 38$  µm was analyzed from the total raster area to reduce the effect of surface B contamination. Reliable SIMS analysis requires steady-state ionization to be attained for  $^{11}\text{B}$  and  $^{30}\text{Si}$ . An initial strategy with indium-mounted samples of no presputtering was performed so as to observe how signals from each element evolved throughout the course of measurement for at least 40 cycles. Stable  $^{11}\text{B}/^{30}\text{Si}$  ratios, indicative of steady-state ionization for both elements, were typically obtained after 10 cycles, and therefore epoxy-mounted samples were measured using a pre-sputter time equivalent to the duration of 10 measurement cycles. Each sample/standard was measured at 3–10 different positions. Data were retained for analysis in which B/Si ratios remained stable (<15% variation) for at least 15 cycles (e.g. Electronic annex EA-2b, c, d, e, g).

NIST glass standards 610 (363 ppm B), 612 (34.9 ppm B), 615 and 614 (1.3 ppm) were used to establish the calibration curve. B concentrations used were obtained from bulk sample analysis as compiled by Jochum et al. (2011). Standards were crushed and sieved (<20 µm) to ensure a porosity and grain size similar to the samples. In indium B/Si ratios of powders were similar to those of solid NIST glass 610 and 612, while for 615/614 ratios of powder gave highly variable measurements due to topography or sample contamination. Therefore, calibration for *T. pseudonana* samples mounted in indium followed the use of powdered NIST 610 and 612, and glass NIST 615  $^{11}\text{B}/^{30}\text{Si}$  ratios (Electronic annex EA-3a). Conversely, stable measurements were successfully obtained for powdered NIST 610, 612 and 614 standards mounted in epoxy and therefore, calibration of epoxy-mounted samples (*T. weissflogii*) was conducted exclusively with powdered standards.

We retain analyses in which stable (<15% variation over 15 cycles) B/Si ratio was reached (e.g. Electronic annex EA-2a, f). These criteria were met by a set of 6 samples of *T. pseudonana* and 4 samples of *T. weissflogii*. Stability of  $^{11}\text{B}/^{30}\text{Si}$  was notably improved for measurements performed in epoxy, both for samples as for powdered NIST standards. In fact, stability criteria were met by all measured samples and standards after 20 cycles of measurement, instead of the minimum of 40 cycles needed for measurements performed on indium. The higher instability of powdered standards (especially 612 and 614) on indium compared to epoxy shows that the signal instability observed for indium-mounted samples from *T. pseudonana* is not due to sample heterogeneity but possibly to the nature of sample-beam interaction and sample topography.

The reproducibility of the B concentration from multiple spots during the same session was different for each sample, possibly dependent on factors such as topography of the

powder and heterogeneous surface charging. Relative standard errors ranged from <1% to ~20%.

#### 2.4.2. LA-ICPMS

A Photon Machines Analyte G2 laser ablation system (Photon Machines, Inc., Redmond, USA) was employed for all laser ablation experiments of the opal samples mounted in Struers epoxy. Resin media was preferred to indium because it penetrates the spaces between the grains of the powder and reduces porosity, promoting more homogeneous ablation. The system uses a 193 nm ArF\* Excimer laser with 5 ns pulse duration. The energy density was set to 8.7 J/cm<sup>2</sup> in all experiments with a spot size of nominally 85 µm. The instrument further features a HelEx® two-volume ablation cell providing aerosol washout times of <10 s for a signal drop of 3 orders of magnitude. The aerosol was transported to the ICPMS through PTFE tubing of approximately 1.5 m length and 4 mm internal diameter, using He as carrier gas fed to the larger compartments of the ablation cell, and He and Ar as carrier gas fed to the internal cup cell. The total He and Ar carrier gas flow rates were held constant at 1.2 and 0.1 l/min, respectively.

An Agilent 7700cx ICP-Quadrupole MS (Tokyo, Japan) was used as detection system. The aerosol was mixed with an Ar make-up gas directly before the central channel of the ICP. The Ar make-up gas was optimized for sensitivity and robust ICP operation conditions (Wang et al., 2006), obtaining a value around 0.75 l/min. The ion optic was adjusted to maximum sensitivity and balanced mass response while ablating NIST 612. The optimization was done out while monitoring <sup>7</sup>Li<sup>+</sup>, <sup>133</sup>Cs<sup>+</sup>, <sup>232</sup>Th<sup>+</sup>, <sup>238</sup>U<sup>+</sup> and <sup>232</sup>Th<sup>16</sup>O<sup>+</sup> ion signal intensities. Plasma robustness was monitored via the <sup>232</sup>Th<sup>16</sup>O<sup>+</sup>/<sup>232</sup>Th and the <sup>238</sup>U/<sup>232</sup>Th intensity ratios. ThO<sup>+</sup>/Th<sup>+</sup> intensity ratios were always below 0.5% and the Ar make-up gas was adjusted to ensure a <sup>238</sup>U<sup>+</sup>/<sup>232</sup>Th<sup>+</sup> intensity ratio of less than 1.2. Additionally, the cross calibration of the pulse and analogue stages of the SEM detector (PA-factor) was carried out daily to ensure a linear response of the instrument of >8 orders of magnitude.

Ion signals from <sup>11</sup>B and <sup>29</sup>Si were acquired using integration times of 100 ms and 20 ms, respectively, at 3–25 different locations and using tracks of 85 µm diameter and ~500 µm longitude (raster mode of the LA unit) within each opal sample. A speed of 4 µm/s and a laser repetition rate of 10 Hz were applied. Data for every sample were obtained during 150 s, using the first 30 s to collect the background ICPMS ion signal of each isotope, then ablating the sample during 110 s to get the LA ICPMS ion signal, and finally allowing a wash out time of 10 s after the last laser shot. <sup>11</sup>B and <sup>29</sup>Si ICPMS background ion signal remained low (<~80 and <~2100 counts, respectively).

The abundance of frustules at the surface of the resin was very heterogeneous possibly due to floating of the low density powder when epoxy is still liquid. Consequently, <sup>11</sup>B and <sup>29</sup>Si counts for every track varied greatly depending on the location of the sample that was ablated. For the most superficial samples, <sup>11</sup>B reached as high as ~3 × 10<sup>3</sup> counts and <sup>29</sup>Si as high as 1 × 10<sup>6</sup> counts. In most cases, lower sample concentration in the surface of the resin

Table 1

Calibration equations at the beginning (*i*) and end (*f*) of every LA-ICPMS session using powdered <20 µm NIST 612 and NIST 614. \*Denotes calibration curve calculated for middle-end session as no calibration curve was possible at the end of 28/10/2011 session. NP = Not possible to calculate end calibration for 29/06/2012 session. The longest sessions (28/11/2011 and /20/03/2012) have the longest cumulative drift in the calibration.

Date	Calibration <sub><i>i</i></sub>	Calibration <sub><i>f</i></sub>	Type of analysis
27/10/2011	$y = 3934.5x$	$y = 4144.6x$	Raster
28/10/2011	$y = 4187.6x$	$y = 4281.8x^*$	Raster
07/11/2011	$y = 4024.0x$	$y = 4140.8x$	Raster
28/11/2011	$y = 3490.1x$	$y = 4038.9x$	Raster
20/03/2012	$y = 3988.9x$	$y = 4434.0x$	Raster
29/06/2012	$y = 6553.9x$	NP	Single spot

did not seem to affect B/Si ratios, except for some tracks in which sample was so diluted that <sup>11</sup>B counts were only twice as high as in the resin blank, in which case the measurements were not retained. For those samples that were not on the surface of the epoxy, we performed ablation in one spot (ø = 60 µm, 1000 shots during 100 s) using the same frequency and fluence applied for previous analysis, with the aim of profiling deep enough to reach embedded frustules.

Resin blank depended on its preparation and varied from session to session. Both <sup>11</sup>B and <sup>29</sup>Si counts remained low (<~100 and <~2500, respectively) and decreased within every session in a proportional way, possibly due to a decrease in sensitivity. Average resin blanks measured at the start and end of each run were linearly interpolated for every measurement when possible and subtracted from <sup>11</sup>B and <sup>29</sup>Si of every data obtained for each track. The median of <sup>11</sup>B/<sup>29</sup>Si within the stable region of each analysis was calculated so as to exclude high and low spikes from the resulting ratios (e.g. Electronic annex EA-4a, b). Stable ablation generates predominantly small particles (nm sized) which are effectively ionized in the plasma. In contrast, unstable regions of analysis can result from poor coupling of the laser to the sample surface and uneven ablation which yields a higher proportion of large (µm sized) particles that are incompletely ionized in the plasma and may experience elemental fractionation. Poor coupling is ubiquitous at the onset of ablation, and can arise subsequently due to changes in surface topography. Unstable parts of the signal are typically omitted from analysis because they are believed to yield non-reproducible analytical data (Kosler, 2008). Relative standard error of replicate laser tracks on the same sample ranges from <1% to 20%.

The calibration curve was established using <sup>11</sup>B/<sup>29</sup>Si ratios from powdered NIST 612 and 614, containing 34.9 ppm and 1.3 ppm B, respectively, obtained from bulk sample analysis as compiled by Jochum et al. (2011). Powdered standards were mounted with the same technique as samples. Calibration was successful on powdered NIST both with raster and single spot ablation modes. Whenever possible, a calibration curve was calculated at the beginning and end of the analysis and B content was obtained from

the linearly interpolated slope for every measurement (Table 1). B/Si ratios from powdered NIST 612 were different to those from glass, while ratios remained more similar for NIST 614 (Electronic annex EA-3b).

## 2.5. Data treatment

Because standards were matched in major element matrix (SiO<sub>2</sub>), size class (<20 µm) and mounting method, we expected high reproducibility of B content for samples analyzed repeatedly in different analytical sessions. For this reason we did not devise an opal consistency standard of large volume to be run in each session. However, we found that samples run on multiple sessions often yielded slightly different B content. We conclude that compared to the NIST glass powders, the different water content of opal (~10%), as well as particle shape and precise size, which depends on the species analyzed, could have resulted in offsets similar to those described previously for LA-ICPMS analyses, and attributed to non-matrix matched standards (e.g. Hill et al., 2012). This may have been especially pronounced for *T. pseudonana* analysis via ion probe, whose calibration followed the use of 615 in polished disk rather than powdered form. To deal with this problem, previous workers have reported LA-ICPMS data as anomalies from the mean measured concentrations (e.g. Hill et al., 2012). We adapt a similar approach to homogenize the data from multiple analytical sessions.

Nearly all of our analytical sessions contain 3 samples which were also analyzed in multiple other sessions, including those by other instruments. For each session, we calculate the mean B content of the three samples common to other sessions, termed the reference sample set. Then for all the samples within the session, we calculate the B anomaly with respect to the mean calculated for the reference sample set. We then calculate a global mean for the reference sample set, averaged over all the sessions in which it was analyzed. We add this mean to the anomaly for each sample to estimate a B content homogenized for differences in the absolute values obtained in different sessions. The calculation is delineated in Electronic annex EA-5.

We have been able to establish one reference sample set for the species *T. weissflogii* and another for *T. pseudonana*, which incorporates a total of seven of the nine analytical sessions and measurements of all but two of the 12 samples. In five out of seven samples in which standard deviations of raw B concentrations were >0.9 ppm, homogenization of data yielded lower standard deviations. We infer that this data treatment has compensated, in part, for the non-matrix matched standard effect (Electronic annex EA-6). We subsequently illustrate the homogenized as well as the raw data in figures. For the sessions in which we do not have the reference set, we have compared single samples analyzed on multiple dates. For example, the replicate measurement of *T. weissflogii* cultured at pH 7.54 using spot analysis yielded comparable B/Si ratios and B content as raster analysis from a previous session.

## 3. RESULTS

### 3.1. Silicification

Si quotas in *T. pseudonana* ranged from 1.2 to 4.6 pg Si/cell, while larger cells from *T. weissflogii* also had higher Si quotas (25 to 58 pg Si/cell). In *T. weissflogii*, growth rates were <1.0/day and Si quotas decrease as growth rate increases ( $r = -0.899$ ;  $p = 0.015$ ;  $n = 6$ , Fig. 2b, Table 2b). In the faster growing *T. pseudonana* (1.0–1.54/day) there is no significant correlation between Si quotas and growth rates (Fig. 2a, Table 2a).

While Si quotas were higher for *T. weissflogii*, Si/C ratios were similar for both species. The Si/C ratio was positively correlated with pH in both species (Fig. 3a, b; *T. pseudonana*:  $r = 0.768$ ,  $p = 0.009$ ,  $n = 10$ ; *T. weissflogii*:  $r = 0.727$ ,  $p = 0.101$ ,  $n = 6$ ). pH was weakly anticorrelated with C quotas in *T. pseudonana* ( $r = -0.492$ ;  $p = 0.149$ ;  $n = 10$ ), while no evidence of correlation was found between pH and Si quotas for this species ( $r = 0.136$ ,  $p = 0.707$ ;  $n = 10$ ). Conversely, none of the correlations between pH and Si or C quotas for *T. weissflogii* were found to be significant (pH vs. Si quotas:  $r = 0.646$ ;  $p = 0.166$ ;  $n = 6$ ; pH vs. C quotas:  $r = -0.087$ ;  $p = 0.870$ ;  $n = 6$ ) (Table 2a, b).

### 3.2. Boron content

#### 3.2.1. B/Si and B content in *T. pseudonana* cultured at varying light intensity

Growth rates from some *T. pseudonana* cultures were regulated by varying light intensities. Samples with low (0.44/day) and high growth rates (1.14–1.16/day), cultured at a constant pH of ~8.0 were analyzed via LA-ICPMS and ion probe. Though only these two end-member growth rates were available for analysis, the data suggest B content increasing with growth rate (Fig. 4), both for raw data and homogenized data (raw:  $r = 0.691$ ,  $p = 0.039$ ,  $n = 9$ ; homogenized:  $r = 0.651$ ;  $p = 0.058$ ;  $n = 9$ ).

#### 3.2.2. B/Si and B content in *T. pseudonana* and *T. weissflogii* cultured at varying pH

Homogenized B content in *T. pseudonana* cultured at different pH conditions (7.50–8.63) ranged from 4.3 to 12.4 ppm, while B concentrations in *T. weissflogii* frustules cultured at pH ranging between 7.54 and 8.33, varied between 2.3 and 9.9 ppm. In both species, B content shows a strong positive correlation with pH (Fig. 5a, b). Slight differences in the raw B concentrations observed between sessions and analytical methods did not affect the statistical significance of the positive correlation between these variables, which are similar when regressions were obtained from both the whole set of homogenized data (*T. pseudonana*:  $r = 0.929$ ,  $p = 0.022$ ,  $n = 5$ ; *T. weissflogii*:  $r = 0.892$ ,  $p = 0.042$ ,  $n = 5$ ) (Table 3) and raw data (*T. pseudonana*:  $r = 0.934$ ,  $p = 0.020$ ,  $n = 5$ ; *T. weissflogii*:  $r = 0.878$ ,  $p = 0.050$ ,  $n = 5$ ). Likewise, this trend is statistically significant in raw data from a single analytical approach, despite the slightly lower concentrations of B in *T. pseudonana* obtained with LA-ICPMS, or the wider range in B content (3.3–11 ppm) in *T. weissflogii* via ion probe compared to

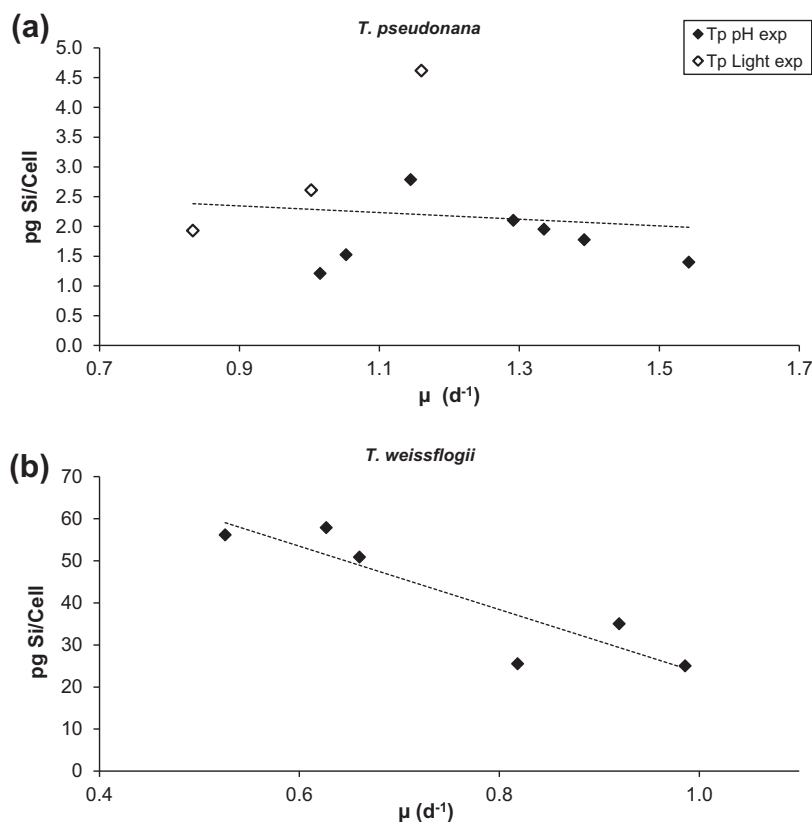


Fig. 2. Si quotas (pg Si/Cell) as a function of growth rate ( $\mu$ ) for (a) *T. pseudonana* cultured at pH varying from 7.41 to 8.63 ( $r = -0.120$ ;  $p = 0.741$ ;  $n = 10$ ) and (b) *T. weissflogii* cultured at pH = 7.44–8.33 ( $r = -0.899$ ;  $p = 0.015$ ;  $n = 6$ ), including both pH (solid) and light (open) experiments from which Si quotas are available.

Table 2

Correlation of pH, photosynthesis  $\text{HCO}_3^-$  uptake, growth rate ( $\mu$ ), Si quotas (pg Si/cell), C quotas (pg C/cell) and Si/C ratios and significance levels (in parentheses) from both light and pH experiments for (a) *T. pseudonana* ( $n = 10$  except when indicated by \*, where  $n = 7$ ) and (b) *T. weissflogii* ( $n = 6$  except when indicated by \*, where  $n = 5$ ). Bold characters reflect significant relationships ( $p < 0.1$ ). *T. pseudonana* light experiment cultured at pH = 8.006 was excluded from the analysis because lack of  $\text{HCO}_3^-$  uptake, Si quotas and Si/C data.

	pH	f ( $\text{HCO}_3^-$ ) (%)	$\mu$	pg Si/cell	pg C/cell	Si/C
(a)						
pH	1					
f ( $\text{HCO}_3^-$ ) (%)	0.057 (0.903)*	1				
$\mu$	0.365 (0.300)	0.477 (0.279)*	1			
pg Si/cell	0.136 (0.707)	-0.148 (0.752)*	-0.120 (0.741)	1		
pg C/cell	-0.492 (0.149)	-0.135 (0.773)*	-0.366 (0.298)	<b>0.552 (0.098)</b>	1	
Si/C	<b>0.768 (0.009)</b>	0.038 (0.936)*	0.304 (0.393)	0.239 (0.507)	<b>-0.657 (0.039)</b>	1
(b)						
pH	1					
f ( $\text{HCO}_3^-$ ) (%)	0.617 (0.268)*	1				
$\mu$	-0.482 (0.333)	<b>-0.944 (0.016)*</b>	1			
pg Si/cell	0.646 (0.166)	<b>0.993 (0.001)*</b>	<b>-0.899 (0.015)</b>	1		
pg C/cell	-0.087 (0.870)	0.786 (0.115)*	-0.234 (0.655)	0.385 (0.451)	1	
Si/C	0.727 (0.101)	<b>0.917 (0.029)*</b>	<b>-0.828 (0.042)</b>	<b>0.907 (0.013)</b>	-0.024 (0.964)	1

LA-ICPS (5.1–8.8 ppm) (Electronic annex EA-7a, b, EA-8a,b; *T. pseudonana* LA-ICPMS:  $r = 0.851$ ,  $p = 0.068$ ,  $n = 5$ ; *T. pseudonana* ion probe  $r = 0.943$ ,  $p = 0.057$ ,  $n = 4$ ; *T. weissflogii* LA-ICPMS:  $r = 0.830$ ,  $p = 0.082$ ,  $n = 5$ ; *T. weissflogii* ion probe  $r = 0.906$ ,  $p = 0.094$ ,  $n = 4$ ) (Electronic annex EA-9).\

The correlation between B content and pH does not result from variations in growth rate, as growth rate remained fairly stable in both diatoms species within the cultured pH conditions and no linear relationship was observed (*T. pseudonana*:  $r = 0.384$ ;  $p = 0.524$ ;  $n = 5$  and *T. weissflogii*:  $r = -0.488$ ;  $p = 0.404$ ;  $n = 5$ ) (Electronic annex EA-7a

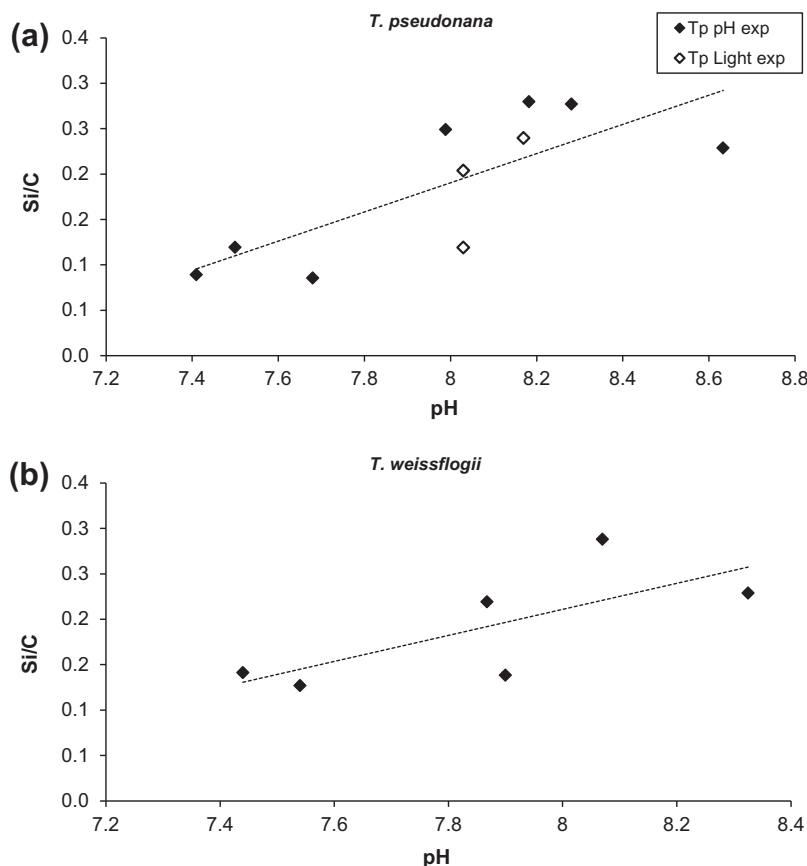


Fig. 3. Increasing trend of Si/C ratio with seawater pH for (a) *T. pseudonana* cultured at pH varying from 7.41 to 8.63 ( $r = 0.768$ ;  $p = 0.009$ ;  $n = 10$ ) and (b) *T. weissflogii* cultured at pH = 7.44–8.33 ( $r = 0.727$ ;  $p = 0.101$ ;  $n = 6$ ), including both pH (solid) and light (open) experiments from which Si and C quotas are available.

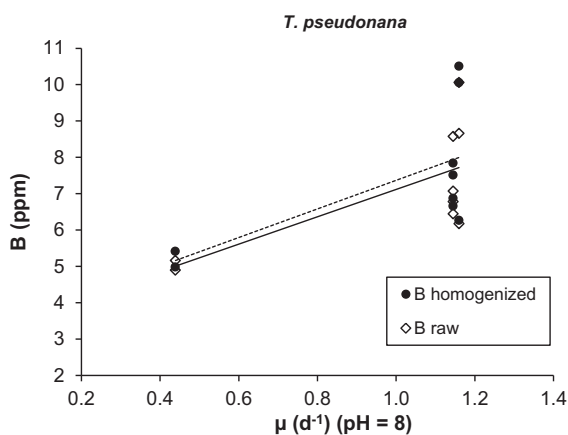


Fig. 4. Homogenized (solid) and raw (open) frustule B content (ppm) as a function of growth rate ( $\mu$ ) from *T. pseudonana* samples cultured at varying light intensities and at a pH of  $\sim 8.0$ . The lower B concentrations at slower growth rates are suggestive of a correlation between variables for both raw data (solid line) ( $r = 0.691$ ,  $p = 0.039$ ,  $n = 9$ ; equation:  $y = 3.763x + 3.353$ ) and homogenized B content (dashed line) ( $r = 0.651$ ;  $p = 0.058$ ;  $n = 9$  equation:  $y = 3.931x + 3.437$ ).

and EA-8a). In accordance with these results, (Crawford et al., 2011) did not find any evidence of a  $\text{CO}_2$ -induced

(pH-induced) variation in growth rate for *T. pseudonana* when culturing  $\sim 100$  generations under  $\text{pCO}_2$  varying between 380 and 760  $\mu\text{atm}$ .

#### 4. DISCUSSION

Diatom opal biomineralization occurs at different cellular conditions and involves different mechanisms compared to calcification and consequently, factors controlling B content may differ from the ones reported for foraminifera, corals and coccolithophorids.

Regardless of the method of analysis (LA-ICPMS or ion probe), seawater pH is strongly positively correlated with B content of both *T. pseudonana* and *T. weissflogii*. Among key factors that might regulate frustule B concentrations are the degree of opal silicification and the mechanism of B uptake, both of which may be, in turn, strongly controlled by seawater pH.

##### 4.1. Degree of frustule silicification

Frustule thickness and cell size are key factors controlling the degree of diatom silicification. Larger cells are more silicified than smaller cells because frustule components are larger and therefore, they have a greater surface area and

hence more Si/cell compared to small cells (Martin-Jézéquel et al., 2000). The latter explains the higher Si quotas observed in *T. weissflogii* ( $\sim 539\text{--}911 \mu\text{m}^2$ ) compared to *T. pseudonana* ( $\sim 70 \mu\text{m}^2$ ). One recognized control on silicification is the cell division rate and indirectly all factors controlling growth rate (Martin-Jézéquel et al., 2000). The observed anticorrelation between silica quotas and growth rate in this work for *T. weissflogii* is in good agreement with the results of various studies, in which growth rate of different species was modulated by means of varying light intensity (Davis, 1976; Taylor, 1985), nitrogen availability and temperature (Durbin, 1977; Furnas, 1978). Under non-limiting Si conditions, Si incorporation depends on the duration of the deposition phase of the cell wall, which is longer if growth rates are slower (Martin-Jézéquel et al., 2000), allowing more Si transport and incorporation per unit of time. However, the lack of an anticorrelation for *T. pseudonana* may reflect greater plasticity in cell size in this species in our experiments, evident in the absence of correlation between Si/C and Si quotas (Table 2a).

In addition to growth rate, the strong positive correlation between pH and Si/C ratios found for both species suggests an important control of pH and/or  $\text{CO}_2$  on the degree of diatom silicification. Si quotas in *T. weissflogii* have been shown to be reduced in cultures grown at  $\text{CO}_2$  concentrations of 370 and 750 ppmv compared to those at 100 ppmv (Milligan et al., 2004). We observe a similar trend in Si quotas in our *T. weissflogii*, reduced Si quotas continuing to even higher  $\text{CO}_2$  concentrations (up to 3000 ppmv) in our lowest pH experiments. This trend of decreased silicification at high  $\text{CO}_2$  and low pH is even more notable when we use the Si/C ratio as the indicator of the degree of silicification, because this controls for variations in cell size. The Si/C ratio of both *T. weissflogii* and *T. pseudonana* is positively correlated to pH, although no correlation was evident between Si quota and pH in *T. pseudonana*.

One function of the silica frustule is maintenance of optimal pH for the enzyme carbonic anhydrase (CA) (Milligan et al., 2004), and the need for the frustule to bolster the efficiency of this enzyme is expected to increase at higher seawater pH and lower  $\text{CO}_2$ . The well-conserved photosynthetic enzyme Ribulose-1,5-biphosphate carboxylase oxygenase (RubisCO) employs dissolved  $\text{CO}_2$  to fix carbon for photosynthesis and has a low affinity for it due to competition with  $\text{O}_2$  at the active site. Consequently, as  $\text{CO}_2$  in seawater decreases (pH increases), RubisCO becomes more inefficient. As an adaptative response to the large decrease in  $\text{CO}_2$  concentrations during the last millions of years, phytoplankton has evolved different carbon concentration mechanisms (CCM) to obtain carbon from the “new”  $\text{CO}_2$ -depleted seawater (Tortell, 2000). Among these CCM is the CA enzyme that catalyzes the equilibrium reaction between  $\text{HCO}_3^-$  and  $\text{CO}_2$  (Milligan et al., 2004; Tachibana et al., 2011), so that the most abundant  $\text{HCO}_3^-$  can be transformed into  $\text{CO}_2$  and there is enough substrate for RubisCO (Tortell et al., 1997; Crawford et al., 2011). This enzyme is widely used by actual marine diatoms, and its activity has been found to be strongly anticorrelated to  $\text{CO}_2$  (Milligan and Morel, 2002; Tortell et al., 2006; Trimborn et al., 2009). The silica frustule of

diatoms is a pH-buffer for the catalytic activity of the CA (Milligan et al., 2004). Therefore, when availability of  $\text{CO}_2$  in seawater decreases (higher pH), cells should be more silicified to enhance  $\text{HCO}_3^-$  to  $\text{CO}_2$  transformation, explaining the direct correlation between Si/C ratios and pH observed here. Supporting this argument, the carbon concentration factor (CCF) obtained from the same *T. weissflogii* cultures as in this study, were found to be positively correlated to pH (Isensee et al., in press), suggesting that pH increases ( $\text{CO}_2$  decreases) force the cell to apply more CCM so as to increase the cellular DIC concentrations compared to external seawater DIC.

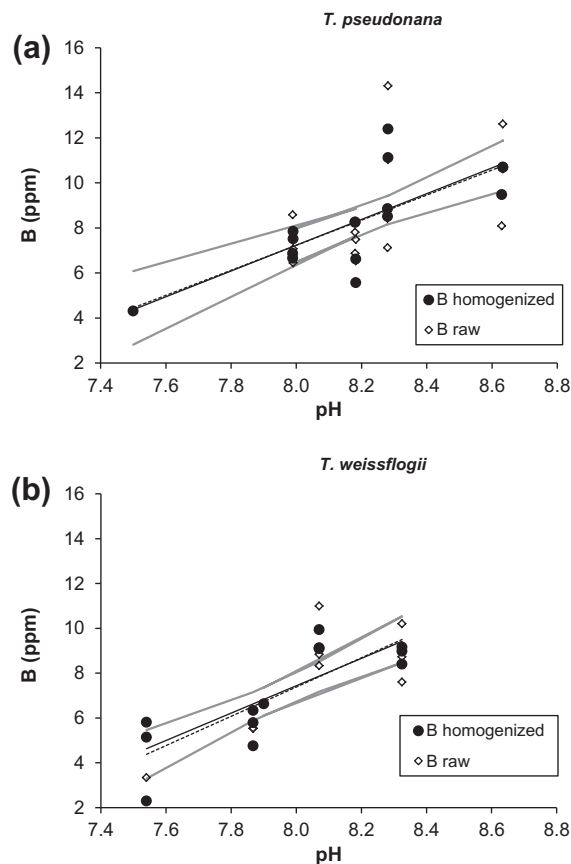


Fig. 5. Homogenized (solid) and raw (open) frustule B content (ppm) from both LA-ICPMS and ion probe analysis in (a) *T. pseudonana* and (b) *T. weissflogii* as a function of seawater pH from samples cultured at varying pH conditions (*T. pseudonana*: pH = 7.50–8.63; *T. weissflogii*: pH = 7.54–8.33). A statistically significant increasing trend of B content with pH is observed in both species for both homogenized and raw B content (*T. pseudonana* homogenized:  $r = 0.747$ ;  $p = 0.0009$ ;  $n = 16$ ; equation:  $y = 5.566x - 37.296$ ; *T. pseudonana* raw:  $r = 0.647$ ;  $p = 0.0067$ ;  $n = 16$ ; equation:  $y = 5.726x - 38.578$  and *T. weissflogii* homogenized:  $r = 0.825$ ;  $p = 0.0005$ ;  $n = 13$ ; equation:  $y = 6.528x - 44.837$ ; *T. weissflogii* raw:  $r = 0.793$ ;  $p = 0.0012$ ;  $n = 13$ ; equation:  $y = 6.098x - 41.342$ ). Linear regressions are shown as dashed (homogenized data) and solid (raw data) lines. Continuous lines indicate 90% confidence intervals of each regression. The slopes of B vs pH regressions are not statistically distinguishable for the two diatom species at the 80% (or higher) confidence level (multiple regression test  $t$ -stat 0.505 for 17 degrees of freedom).

Table 3

Correlation of average homogenized (AH) B content (ppm) obtained from both ion probe and LA-ICPMS measurements with pH, photosynthesis  $\text{HCO}_3^-$  uptake, growth rate ( $\mu$ ), Si quotas (pg Si/cell), C quotas (pg C/cell) and Si/C ratios and significance levels (in parentheses), including only data from pH experiments and from fully-cleaned samples for *T. pseudonana* and *T. weissflogii*.  $n = 5$  except when indicated by \*, where  $n = 4$ . Bold characters reflect significant relationships ( $p < 0.1$ ).

	<i>T. pseudonana</i>	<i>T. weissflogii</i>
	AH B (ppm)	AH B (ppm)
pH	<b>0.929 (0.022)</b>	<b>0.892 (0.042)</b>
f ( $\text{HCO}_3^-$ ) (%)		0.336 (0.664)*
$\mu$	0.311 (0.611)	-0.405 (0.499)
pg Si/cell	-0.262 (0.670)	0.490 (0.402)
pg C/cell	<b>-0.902 (0.036)</b>	-0.671 (0.215)
Si/C	0.693 (0.195)	0.791 (0.111)

The competitive success of diatoms in the ocean of the future depends on numerous factors including ocean circulation and nutrient supply, light availability, ecology of diatom species, modifications of population dynamics, and even grazing intensity. Our results suggest that in addition, the dependence of diatom Si/C ratios on seawater pH ( $\text{CO}_2$ ) has important implications on the marine C cycle, which should be taken into account when assessing the possible responses of the biological pump to increasing atmospheric  $\text{CO}_2$  concentrations. According to our findings, in a future more acidic ocean (Caldeira and Wickett, 2003) diatom requirements of Si per fixed C would be lower, which could contribute to reduced mass of diatom ballast and C export efficiency in Si-replete areas. Conversely, phytoplankton communities of Si-limited regions may tend to be shifted towards a dominance of diatom populations, which if replacing small, poorly-exported cells could enhance the biological pump.

#### 4.2. Mechanism of cellular B uptake

If B transport was constant and decoupled from Si transport, B content in opal might be expected to be diluted to lower concentrations in conditions promoting extensive silicification (higher pH, lower  $\text{CO}_2$  concentrations). However, B is positively correlated with the degree of silicification (Si/C), suggesting that B transport to cell may vary as a function of pH.

B is an essential micronutrient for both plant and animal cells. In plants, B is important for protein, carbohydrate, nucleic acid and phenol metabolism, membrane integrity and function, cell wall synthesis and structure. When B is limited in higher plants, flower development, seed and fruit production, leaf expansion and root elongation are inhibited (Tanaka and Fujiwara, 2008). B has been found to be essential for cyanobacteria, many marine flagellates and diatoms (Loomis and Durst, 1992; Marschner, 1995).

##### 4.2.1. Passive diffusion of neutral boric acid

Passive diffusion of neutral  $\text{B(OH)}_3$  through the bi-lipid cell membrane has been proposed as the exclusive/main form of B uptake by higher plants (Tanaka and Fujiwara,

2008) and coccolithophorids (Stoll et al., 2012) under non-limiting B concentrations, though channel-mediated mechanisms may also be involved both in plant (Dordas and Brown, 2001) and animal cells (Dordas et al., 2000) at low B concentrations. Due to the high permeability of the cell membrane to the neutral  $\text{B(OH)}_3$  (Tanaka and Fujiwara, 2008), concentrations in the cytoplasm and in seawater would be expected to be equal, allowing an equilibrium of  $\text{B(OH)}_3$  in and outside of the bi-lipid layer to be reached (Fig. 6). Active uptake of the charged  $\text{B(OH)}_4^-$  would be, in principle, assumed to be inexistent/negligible, considering the energy this process would entail, and that seawater at pH from 7.4 to 8.8 contains  $\text{B(OH)}_3$  concentrations ranging from 413.54 to 198.46  $\mu\text{M}$  (~48% decrease calculated based on B concentration from (Lee et al., 2010)), which is higher than the non-limiting total B concentration for higher plants such as *Helianthus annuus* (100  $\mu\text{M}$ ) (Dannel et al., 2000). Consequently, B concentrations as  $\text{B(OH)}_3$  in seawater at the studied pH would be enough to provide plant cells with the needed B for their development, and no further mechanism of B acquisition would be needed.

If  $\text{B(OH)}_3$  were to be the exclusive B species taken up by diatoms as well, frustule B content would decrease as pH becomes higher, because  $\text{B(OH)}_3$  concentrations in seawater and thereby passive  $\text{B(OH)}_3$  uptake decrease as pH increases (Fig. 1). Since frustule B content was higher with increased pH, exclusive passive uptake by diatoms of  $\text{B(OH)}_3$  can be ruled out and an active uptake of  $\text{B(OH)}_4^-$ , which increases in abundance with pH, must be the main B source for *T. pseudonana* and *T. weissflogii*.

##### 4.2.2. Active co-transport of bicarbonate ion and borate

Various studies have found that worldwide,  $\text{HCO}_3^-$  uptake accounts for a large part of the C flux in phytoplankton communities and specifically in diatoms (Tortell and Morel, 2002; Cassar et al., 2004; Martin and Tortell, 2006; Tortell et al., 2006).

Since we assume that the B taken up by passive diffusion as  $\text{B(OH)}_3$  in the studied pH range is enough for cell demands, the excess of B observed in frustule might have been transported inside the bi-lipid layer mainly as  $\text{B(OH)}_4^-$ , through the same protein transporters that take up  $\text{HCO}_3^-$  for photosynthesis, as a consequence of a poor selectivity of these similarly-sized molecules that have the same charge.  $\text{B(OH)}_4^-$  protein transporters in higher plants (BOR1) have been found to be phylogenetically related to  $\text{HCO}_3^-$  transport proteins (e.g. BTR1) in animals. Consequently,  $\text{B(OH)}_4^-$  transport in higher plants may involve a similar mechanism of anion transporter coupled to the antiport of a counterion, as happens with kidney and red blood cells (Frommer and von Wiren, 2002). Moreover, Kroth et al. (2008) identified that the genes responsible for  $\text{HCO}_3^-$  transport in the diatom *Phaeodactylum tricorutum* code for three proteins, some of which involve anion antiporters (e.g. Na-dependent anion exchangers and  $\text{Cl}^-/\text{HCO}_3^-$  exchangers) similar to those reported for other organisms. Transporters with unknown functions of other organisms, such as yeast (YNL275w), lie between the phylogenetic clades of sole  $\text{B(OH)}_4^-$  and sole  $\text{HCO}_3^-$  trans-

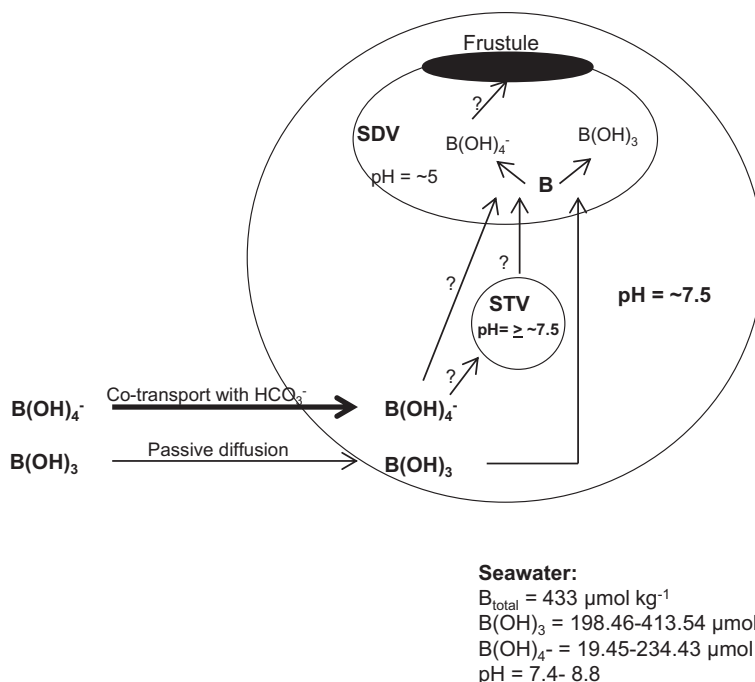


Fig. 6. Schematic model of B content for *T. pseudonana* and *T. weissflogii* (uptake both as  $B(\text{OH})_3$  and  $B(\text{OH})_4^-$ ) as described in Sections 4.2–4.4. Total B,  $B(\text{OH})_3$  and  $B(\text{OH})_4^-$  concentrations based on B/Salinity relationship from Lee et al. (2010). Width of arrows that indicate uptake show that B mainly enters the cell as  $B(\text{OH})_4^-$ . A possible  $B(\text{OH})_4^-$  transport mechanism inside the SDV is through STV and/or less likely directly through the SDV membrane. B species incorporated is unknown but is likely to be  $B(\text{OH})_4^-$  via substitution of a charged  $\text{SiO}^-$  during silicification.

porters (Takano et al., 2002), with the possibility of being able to transport both molecules. Accordingly, from the evolutionary point of view, it is possible that diatom  $\text{HCO}_3^-$  protein transporters have the ability of transporting  $B(\text{OH})_4^-$  as well, as proposed here to explain the observed high B content with increasing pH (Fig. 6).

The correlation between light-regulated growth rate and B content from varying light experiments of *T. pseudonana* may be also explained by a co-transport of  $\text{HCO}_3^-$  and  $B(\text{OH})_4^-$ . Light limitation has been shown to significantly reduce the amount of active C transport to and within the diatom cell, as diagnosed from carbon isotopic composition of organic matter (Cassar et al., 2006). This active C transport was shown to be dominantly as  $\text{HCO}_3^-$  (Hopkinson et al., 2011). Therefore a decreased active uptake of  $\text{HCO}_3^-$  at lower light intensities would imply a lower  $B(\text{OH})_4^-$  transport, which would explain the lower B content in frustules of cells under light-limited growth.

In contrast to passive diffusion of  $B(\text{OH})_3$ ,  $B(\text{OH})_4^-$ / $\text{HCO}_3^-$  transport by the same proteins could explain the observed increase in frustule B content with increasing pH. When seawater  $\text{CO}_2$  concentrations are higher (lower pH),  $\text{HCO}_3^-$  transport for photosynthesis decreases (Martin and Tortell, 2006), whereas  $\text{HCO}_3^-$  use for photosynthesis increases when  $\text{CO}_2$  availability decreases. Measurements of the  $\text{HCO}_3^-$  contribution to photosynthesis from the  $^{14}\text{C}$  disequilibrium technique reveal increasing  $\text{HCO}_3^-$  contribution with increasing pH/decreasing  $\text{CO}_{2\text{aq}}$  in *T. weissflogii* ( $r = 0.970$ ;  $p = 0.001$ ;  $n = 6$ ) (Burkhardt

et al., 2001; Isensee et al., in press). The latter study employed the same culture samples as employed for measurement of B in frustules. Consequently, if B was taken up by diatoms mainly as  $B(\text{OH})_4^-$  through co-transport with  $\text{HCO}_3^-$ , as pH increases and  $\text{HCO}_3^-$  demand increases, more B would be introduced inside the cells and frustule B concentrations would be expected to be higher as well. The 6-fold increase in CCF observed by Isensee et al. (in press) for our *T. weissflogii* cultures gives an insight of the magnitude of increase in  $\text{HCO}_3^-$  uptake with pH, which is not necessarily linear but rather suggests a threshold  $\text{CO}_2$  above which CCMs are not utilized.

In *T. pseudonana*,  $\text{HCO}_3^-$  uptake by the cell has been estimated to account for 50% of C fixation in cells acclimated at pH of 7.9–8.2 ( $\text{CO}_{2\text{aq}}$  of 14–31  $\mu\text{M}$ ) (Trimborn et al., 2009). In experiments with the same strain employed here, the same method indicates that the portion of C fixation supported by  $\text{HCO}_3^-$  increases from 52% at  $\text{CO}_{2\text{aq}}$  of 21  $\mu\text{M}$  (pH = 7.99) to a maximum of 86% at  $\text{CO}_{2\text{aq}}$  of 5.45  $\mu\text{M}$  (pH = 8.21; Isensee et al., in press).

In addition to the higher  $\text{HCO}_3^-$  demand as pH increases,  $B(\text{OH})_4^-/\text{HCO}_3^-$  ratios in seawater might be another factor controlling  $B(\text{OH})_4^-$  uptake and hence, B content. Over the pH range of our cultures, with increasing seawater pH,  $B(\text{OH})_4^-$  increases while  $\text{HCO}_3^-$  decreases, yielding increasing  $B(\text{OH})_4^-/\text{HCO}_3^-$  ratios (Fig. 7), which may in turn increase relative uptake of  $B(\text{OH})_4^-$  vs.  $\text{HCO}_3^-$  even given constant rates of operation of  $\text{HCO}_3^-$  transporters. Consequently, B content in frustules may not

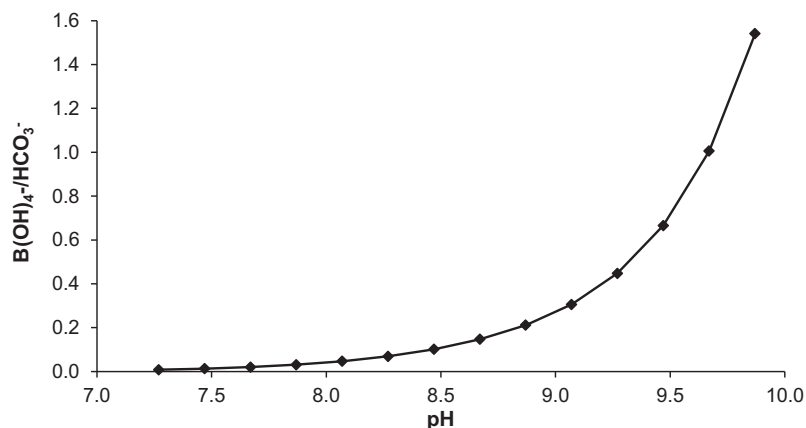


Fig. 7.  $B(OH)_4^-/HCO_3^-$  ratios as a function of pH assuming a salinity of 35 and temperature of 20 °C (Dickson et al., 2007).

only increase with pH due to a higher requirement of  $HCO_3^-$  for photosynthesis, but also due to the increasing  $B(OH)_4^-/HCO_3^-$  ratios of seawater.

#### 4.3. Transport to the silicon deposition vesicle

Whereas  $B(OH)_3$  may enter the SDV by passive diffusion (Fig. 6), understanding the processes involved in the transport of  $B(OH)_4^-$  to the SDV is not straightforward, since not even uptake mechanisms of substances contributing to silicification (e.g. silicic acid, proteins) are yet clear. B transport from the site of uptake to the SDV may occur through a variety of mechanisms. The simplest plausible mechanism might be through permeable-protein-mediated diffusion of  $B(OH)_4^-$  ions that follow the concentration gradient across a negatively-charged SDV membrane (uniport) (Fig. 6), as proposed for the BOR1 transporter in higher plants (Frommer and von Wiren, 2002). However, because pH regulating mechanisms of the SDV are not understood, the charge of the membrane is unknown. Additionally, due to the acidic pH inside this vesicle, the concentration of  $H^+$  inside it should be kept high. A constant  $H^+$  export outside the membrane via e.g.  $H^+$ -ATPases, which would enable it to be negatively charged (Frommer and von Wiren, 2002), is therefore unlikely.

A further mechanism may involve silicic acid transport mechanisms through  $B(OH)_4^-$  uptake by silicon transport vesicles (STV) from the cytoplasm (Fig. 6). Vrieling et al. (1999) proposed that silicic acid taken up by diatoms may be enclosed in STV, whose pH is assumed to be relatively high ( $> \sim 7.5$ - $pH_{cytoplasm}$ ) to avoid monomer polymerization, suggesting some kind of pH regulation inside the vesicle. One of the main pH regulation mechanisms in kidney and red blood cells implies the antiport of  $Cl^-$  and  $HCO_3^-$  anions though Na-dependent and Na-independent transport mechanisms (Alper et al., 2002). Na-dependent  $Cl^-/HCO_3^-$  antiport imports  $HCO_3^-$  and  $Na^+$  and exports  $H^+$  and  $Cl^-$ , promoting alkalosis, as one  $H^+$  is exported outside the cell and the  $HCO_3^-$  imported neutralizes a  $H^+$  in the cytoplasm. Conversely, Na-independent  $Cl^-/HCO_3^-$  antiport acidifies the cytoplasm through the export of  $HCO_3^-$  anions, increasing the concentration of free  $H^+$

in the cytoplasm (Tepel et al., 1998) (Fig. 8a). Analogously, one of the mechanisms of pH regulation in diatom STV, which would promote alkalosis and prevent silicic acid autopolymerization, may involve  $B(OH)_4^-$  import to the STV, either coupled to the antiport of  $Cl^-$  anions through Na-dependent transporters, with a resulting  $H^+$  expulsion and a  $H^+$  neutralization inside the vesicle (Fig. 8c), or by a direct counter-transport of  $B(OH)_4^-$  and  $H^+$  (Fig. 8d). Similar transport mechanisms of  $B(OH)_4^-$  for BOR1 were proposed by Frommer and von Wiren (2002), with the difference that higher plants transport  $B(OH)_4^-$  to the xylem (Fig. 8b) to redistribute it and use it for physiological needs and diatoms may introduce this anion to STV as part of the pH-regulating machinery of this vesicle, analogously to the way kidney cells do. Moreover, even though B is needed for cell wall structure and synthesis in higher plants, it may become toxic when concentrations are high (Tanaka and Fujiwara, 2008). Consequently, a further reason for which diatoms may take up  $B(OH)_4^-$  ions into STV, is to remove this excess of B from the cytosol, where organic-living parts of the cell are located and may be affected by necrosis or chlorosis, and place it in their inorganic-dead matrix, i.e. within the opal (Fig. 8c, d).

#### 4.4. B incorporation in diatom opal

In carbonates,  $B(OH)_4^-$  has been proposed to be the main form of B incorporated, presumably by substitution for  $HCO_3^-$ , regardless of the biochemical (or abiogenic) pathways of mineral deposition (Hemming and Hansen, 1992; Hemming et al., 1995, 1998; Sanyal et al., 2000). In opal, the form of B incorporated is not certain but we propose that it may be via substitution of  $B(OH)_4^-$  for a negatively-charged  $SiO^-$  that forms during polymerization (Vrieling et al., 1999; Kröger et al., 2000). Although opal is not strictly crystalline, it shows lattice ordering on short length scale and thus the material properties, rather than biomineralization pathways, may define the B species incorporated. To date, preliminary results showing low B isotopic composition in sponge opal suggests that borate may be fixed in the opal lattice (Eggins et al., 2004; de León et al., 2009). Though  $\delta^{11}B$  is likely to be controlled by the material

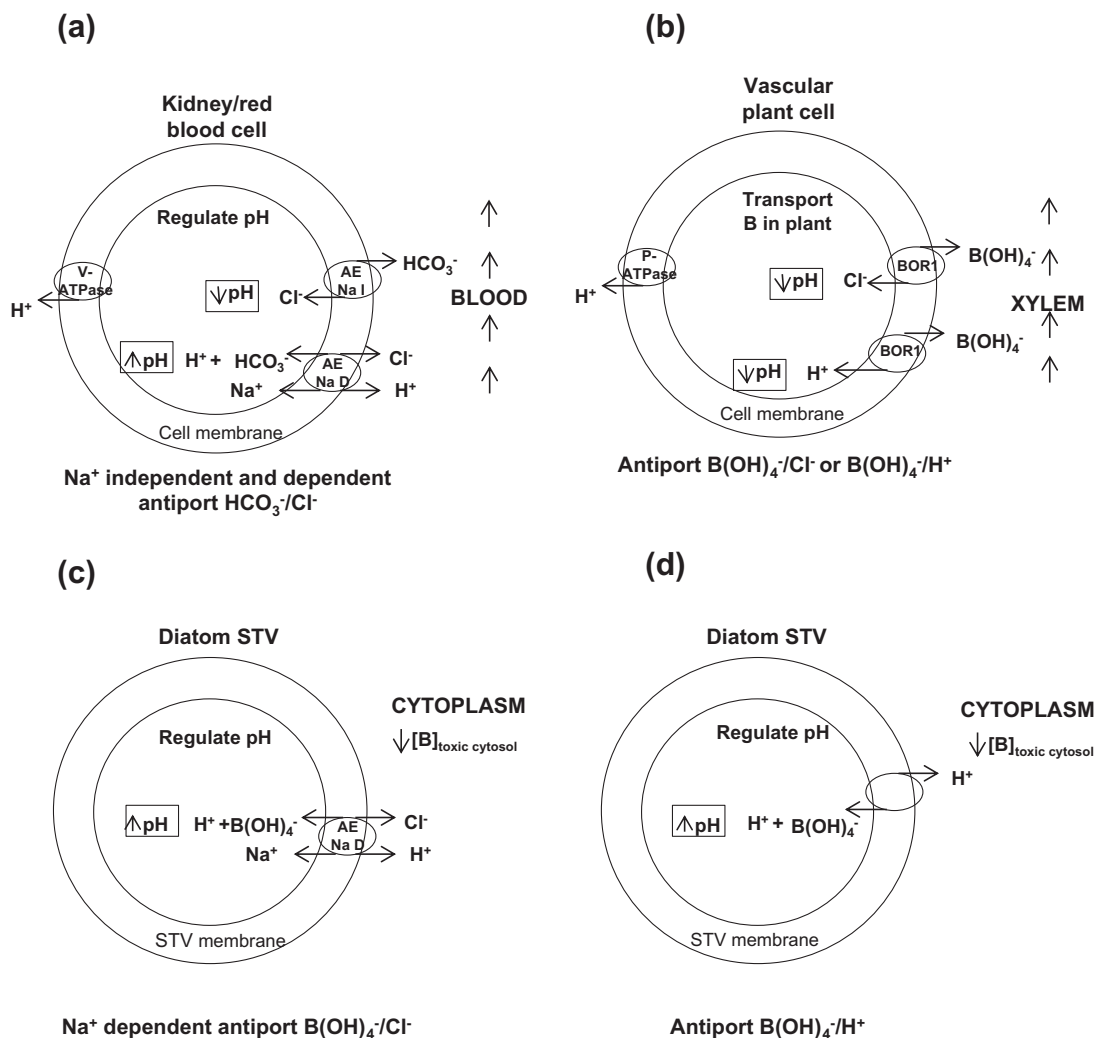


Fig. 8. Similar anion transport mechanisms (antiport) involving phylogenetically related transporters in (a) Na independent (I) and Na dependent (D) anion exchanger (AE) in kidney and red blood cells ( $\text{HCO}_3^-/\text{Cl}^-$  transporters to regulate pH) and (b) BOR 1 transporter in vascular plant cells ( $\text{B(OH)}_4^-$  transport and distribution in plant). An analogous anion transport mechanism as for (a) and (b) for  $\text{B(OH)}_4^-$  uptake inside STV, as part of the pH regulation machinery that promotes alkalosis in the vesicle and/or to reduce B concentrations in the cytoplasm that may become toxic and produce chlorosis/necrosis, is proposed for diatom cells: (c) Na dependent (D) antiport of  $\text{B(OH)}_4^-/\text{Cl}^-$  and (d) Antiport of  $\text{B(OH)}_4^-$  and  $\text{H}^+$ .

properties, there are differences in biosilicification mechanisms and the biomineral ultrastructure between diatom and sponge opal (Schröder et al., 2005). If borate was the main fixed species, B concentrations observed here would imply a high affinity of opal to incorporate  $\text{B(OH)}_4^-$  and suggest a large  $\text{B(OH)}_4^-$  partitioning coefficient, since at the acidic pH of  $\sim 5$  inside the SDV, B speciation would result in dominant  $\text{B(OH)}_3$  concentrations. Moreover, changes in pH at the site of biomineralization are a negligible source of variation in frustule B content as pH here is strictly regulated by diatoms for efficient silicification.

## 5. CONCLUSIONS

Analysis of B/Si ratios in *T. pseudonana* and *T. weissflogii* by means of both LA-ICPMS and ion probe, suggest

that pH is the key factor controlling B content in diatom frustules, likely by both direct seawater chemistry such as the seawater  $\text{B(OH)}_4^-/\text{HCO}_3^-$  ratio, and by physiologically regulated mechanisms such as cellular  $\text{B(OH)}_4^-$  uptake during  $\text{HCO}_3^-$  acquisition.

Many factors may contribute to future modification of phytoplankton communities and C export efficiency in a more acidic ocean, and among these we must consider the pH ( $\text{CO}_2$ )-dependency of the degree of silicification of diatoms. Contrary implications on the biological pump and C export efficiencies would be expected in Si-rich (decreased C export) and Si-limited regions (increased biological pump efficiency) due to the lower Si requirements per C fixed in a more acidic ocean.

Though  $\text{B(OH)}_3$  may be a B supply for the cell, as occurs for higher plants, animals and coccolithophorids, B uptake

in diatoms may occur mainly via co-transport of  $\text{B(OH)}_4^-$  and  $\text{HCO}_3^-$  through a protein transporter that is able to take up both molecules. We hypothesize that both the increasing  $\text{HCO}_3^-$  cell demand and  $\text{B(OH)}_4^-/\text{HCO}_3^-$  ratios with increasing pH, control  $\text{B(OH)}_4^-$  uptake in the cells and ultimately, frustule B content. Though unknown, transport from the site of uptake to the site of silicification may occur via STV by several mechanisms. Successful future measurements of diatom opal B isotopic composition could elucidate the incorporated B species and test some of the proposed acquisition mechanisms.

Since frustule B content may depend mainly on  $\text{B(OH)}_4^-/\text{HCO}_3^-$  co-transport, the determination of B concentrations in fossil diatoms may as well be used to assess the importance of  $\text{HCO}_3^-$  transport and use for photosynthesis in diatoms from the past, which may, in turn, give insights of the evolution of diatom C-acquiring strategies and adaptation to changing pH and  $\text{CO}_2$  conditions.

## 6. AUTHOR CONTRIBUTIONS

K.I and L.M.M cultured the diatoms; L.M.M modified cleaning protocol for small sample size and cleaned samples; A.M.V and L.M.M developed mounting protocol and mounted the samples; H.M.S and L.M.M conducted the ion probe measurements under direction of N.S, B.M; L.M.M conducted LA-ICPMS measurements under direction of J.P, C.G; H.M.S conceived the idea of B as an indicator of pH/diatom physiology; L.M.M and H.M.S wrote the paper.

## ACKNOWLEDGEMENTS

This work was funded by the European Community under the project ERC-STG-240222-PACE. We thank Damian L. Arévalo-Martínez for helpful suggestions and discussion during the writing of the manuscript and Juan Argüelles for his advice and ideas concerning the cellular pH regulating mechanisms.

## APPENDIX A. SUPPLEMENTARY DATA

Supplementary data associated with this article can be found, in the online version, at <http://dx.doi.org/10.1016/j.gca.2013.06.011>.

## REFERENCES

- Alper S. L., Darman R. B., Chernova M. N. and Dahl N. K. (2002) The AE gene family of  $\text{Cl}^-/\text{HCO}_3^-$  exchangers. *J. Nephrol.* **15**, S41–S53.
- Bartoli G., Hönisch B. and Zeebe R. E. (2011) Atmospheric  $\text{CO}_2$  decline during the Pliocene intensification of Northern Hemisphere glaciations. *Paleoceanography* **26**, PA4213. <http://dx.doi.org/10.1029/2010PA002055>.
- Bentov S., Brownlee C. and Erez J. (2009) The role of seawater endocytosis in the biomineralization process in calcareous foraminifera. *Proc. Natl. Acad. Sci. U.S.A.* **106**, 21500–21504.
- Burkhardt S., Amoroso G., Riebesell U. and Sültemeyer D. (2001)  $\text{CO}_2$  and  $\text{HCO}_3^-$  uptake in marine diatoms acclimated to different  $\text{CO}_2$  concentrations. *Limnol. Oceanogr.* **46**, 1378–1391.
- Caldeira K. and Wickett M. E. (2003) Oceanography: anthropogenic carbon and ocean pH. *Nature* **425**, 365–365.
- Cassar N., Laws E. A., Bidigare R. R. and Popp B. N. (2004) Bicarbonate uptake by Southern Ocean phytoplankton. *Global Biogeochem. Cycles* **18**, GB2003.
- Cassar N., Laws E. A. and Popp B. N. (2006) Carbon fractionation by the marine diatom *Phaeodactylum tricornerutum* under nutrient- and light-limited growth conditions. *Geochim. Cosmochim. Acta* **70**, 5323–5335.
- Crawford K. J., Raven J. A., Wheeler G. L., Baxter E. J. and Joint I. (2011) The response of *Thalassiosira pseudonana* to long-term exposure to increased  $\text{CO}_2$  and decreased pH. *PLoS ONE* **6**, e26695.
- Dannel F., Pfeffer H. and Römheld V. (2000) Characterization of root boron pools, boron uptake and boron translocation in sunflower using the stable isotopes  $^{10}\text{B}$  and  $^{11}\text{B}$ . *Funct. Plant Biol.* **27**, 397–405.
- Davis C. O. (1976) Continuous culture of marine diatoms under silicate limitation. II. Effect of light intensity on growth and nutrient uptake of *Skeletonema costatum* 1,2. *J. Phycol.* **12**, 291–300.
- de León A., Willie M., Eggins S. M. and Ellwood M. J. (2009) The boron geochemistry of siliceous sponges. *American Geophysical Union, Fall Meeting, San Francisco*. #PP11C-1325 (poster).
- Dickson A. G., Sabine C. L. and Christian J. R. (2007) Guide to best practices for ocean  $\text{CO}_2$  measurements. *PICES Spec. Publ.* **3**, 191.
- Dordas C. and Brown P. H. (2001) Evidence for channel mediated transport of boric acid in squash (*Cucurbita pepo*). *Plant Soil* **235**, 95–103.
- Dordas C., Chrispeels M. J. and Brown P. H. (2000) Permeability and channel-mediated transport of boric acid across membrane vesicles isolated from squash roots. *Plant Physiol.* **124**, 1349–1361.
- Dugdale R. C. and Wilkerson F. P. (1998) Silicate regulation of new production in the equatorial Pacific upwelling. *Nature* **391**, 270–273.
- Durbin E. G. (1977) Studies on the autoecology of the marine diatom *Thalassiosira nordenskiöldii*. II. The influence of cell size on growth rate, and carbon, nitrogen, chlorophyll *a* and silica content I. *J. Phycol.* **13**, 150–155.
- Eggins S. M., Ellwood M., McCulloch M. and Kelly M. (2004) Silica sponges—archives of palaeoseawater  $\text{pCO}_2$ ? *Research School of Earth Sciences. Annual Report*, The Australian National University.
- Elzenga J. T. M., Prins H. B. A. and Stefels J. (2000) The role of extracellular carbonic anhydrase activity in inorganic carbon utilization of *Phaeocystis globosa* (Prymnesiophyceae): a comparison with other marine algae using the isotopic disequilibrium technique. *Limnol. Oceanogr.* **45**, 372–380.
- Fietzke J., Heinemann A., Taubner I., Böhm F., Erez J. and Eisenhauer A. (2010) Boron isotope ratio determination in carbonates via LA-MC-ICP-MS using soda-lime glass standards as reference material. *J. Anal. At. Spectrom.* **25**, 1953–1957.
- Frommer W. B. and von Wiren N. (2002) Plant biology – Ping-pong with boron. *Nature* **420**, 282–283.
- Furnas M. (1978) Influence of temperature and cell size on the division rate and chemical content of the diatom *Chaetoceros curvisetum* Cleve. *J. Exp. Mar. Biol. Ecol.* **34**, 97–109.
- Hemming N. G. and Hansen G. N. (1992) Boron isotopic composition and concentration in modern marine carbonates. *Geochim. Cosmochim. Acta* **56**, 537–543.
- Hemming N. G., Reeder R. J. and Hanson G. N. (1995) Mineral-fluid partitioning and isotopic fractionation of boron in

- synthetic calcium carbonate. *Geochim. Cosmochim. Acta* **59**, 371–379.
- Hemming N. G., Reeder R. J. and Hart S. R. (1998) Growth-step-selective incorporation of boron on the calcite surface. *Geochim. Cosmochim. Acta* **62**, 2915–2922.
- Hill T. M., LaVigne M., Spero H., Guilderson T., Gaylord B. and Clague D. (2012) Variations in seawater Sr/Ca recorded in deep-sea bamboo corals. *Paleoceanography* **27**, PA3202. <http://dx.doi.org/10.1029/2011PA002260>.
- Hopkinson B. M., Dupont C. L., Allen A. E. and Morel F. M. M. (2011) Efficiency of the CO<sub>2</sub>-concentrating mechanism of diatoms. *Proc. Natl. Acad. Sci. U.S.A.* **108**, 3830–3837.
- Horn M. G., Robinson R. S., Rynearson T. A. and Sigman D. M. (2011) Nitrogen isotopic relationship between diatom-bound and bulk organic matter of cultured polar diatoms. *Paleoceanography* **26**, PA3208. <http://dx.doi.org/10.1029/2010PA002080>.
- Hu Z., Hu S., Gao S., Liu Y. and Lin S. (2004) Volatile organic solvent-induced signal enhancements in inductively coupled plasma-mass spectrometry: a case study of methanol and acetone. *Spectrochim. Acta, Part B* **59**, 1463–1470.
- Isensee K., Erez J. and Stoll H. (in press) Detection of a variable internal C<sub>i</sub> pool in *Thalassiosira weissflogii* (Heterokontophyta) and *Emiliania huxleyi* (Haptophyta) in response to changes in the seawater carbon system. *J. Phycol.* DOI: 10.1111/jppl.12096
- Iversen M. H. and Ploug H. (2010) Ballast minerals and the sinking carbon flux in the ocean: carbon-specific respiration rates and sinking velocities of macroscopic organic aggregates (marine snow). *Biogeosci. Discuss.* **7**, 3335–3364.
- Jochum K. P., Weis U., Stoll B., Kuzmin D., Yang Q., Raczek I., Jacob D. E., Stracke A., Birbaum K., Frick D. A., Günther D. and Enzweiler J. (2011) Determination of Reference Values for NIST SRM 610–617 Glasses Following ISO Guidelines. *Geo-stand. Geoanal. Res.* **35**, 397–429.
- Keller M. D., Selvin R. C., Claus W. and Guillard R. R. L. (1987) Media for the culture of oceanic ultraphytoplankton. *J. Phycol.* **23**, 633–638.
- Kosler J. (2008) Laser ablation sampling strategies for concentration and isotope ratio analyses by ICP-MS. In *Laser Ablation ICP-MS in the Earth Sciences: Current Practices and Outstanding Issues* (ed. P. Sylvester). Centre for Geobiology and Department of Earth Science, Bergen, pp. 79–92.
- Kröger N., Deutzmann R., Bergsdorf C. and Sumper M. (2000) Species-specific polyamines from diatoms control silica morphology. *Proc. Natl. Acad. Sci. U.S.A.* **97**, 14133–14138.
- Kroth P. G., Chiovitti A., Gruber A., Martin-Jezequel V., Mock T., Parker M. S., Stanley M. S., Kaplan A., Caron L., Weber T., Maheswari U., Armbrust E. V. and Bowler C. (2008) A model for carbohydrate metabolism in the diatom *Phaeodactylum tricornutum* deduced from comparative whole genome analysis. *PLoS ONE* **3**, e1426.
- Langer G., Geisen M., Baumann K. H., Klas J., Riebesell U., Thoms S. and Young J. R. (2006) Species-specific responses of calcifying algae to changing seawater carbonate chemistry. *Geochim. Geophys. Geosyst.* **7**.
- Langer G., Nehrke G., Thoms S. and Stoll H. (2009) Barium partitioning in coccoliths of *Emiliania huxleyi*. *Geochim. Cosmochim. Acta* **73**, 2899–2906.
- Lee K., Kim T.-W., Byrne R. H., Millero F. J., Feely R. A. and Liu Y.-M. (2010) The universal ratio of boron to chlorinity for the North Pacific and North Atlantic oceans. *Geochim. Cosmochim. Acta* **74**, 1801–1811.
- Loomis W. D. and Durst R. W. (1992) *Chemistry and biology of boron*. BioFactors (Oxford, England) **3**, pp. 229–239.
- Marschner H. (1995) *Mineral nutrition of higher plants*, second ed. Academic, San Diego, CA.
- Martin-Jézéquel V., Hildebrand M. and Brzezinski M. A. (2000) Silicon metabolism in diatoms: implications for growth. *J. Phycol.* **36**, 821–840.
- Martin C. L. and Tortell P. D. (2006) Bicarbonate transport and extracellular carbonic anhydrase activity in Bering Sea phytoplankton assemblages: results from isotope disequilibrium experiments. *Limnol. Oceanogr.* **51**, 2111–2121.
- Milligan A. J. and Morel F. M. M. (2002) A proton buffering role for silica in diatoms. *Science* **297**, 1848–1850.
- Milligan A. J., Varela D. E., Brzezinski M. A. and Morel F. M. M. (2004) Dynamics of silicon metabolism and silicon isotopic discrimination in a marine diatom as a function of CO<sub>2</sub>. *Limnol. Oceanogr.* **49**, 322–329.
- Nelson D. M., Treguer P., Brzezinski M. A., Leynaert A. and Queguener B. (1995) Production and dissolution of biogenic silica in the ocean – revised global estimates, comparison with regional data and relationship to biogenic sedimentation. *Global Biogeochem. Cycles* **9**, 359–372.
- Ploug H., Iversen M. H., Koski M. and Buitenhuis E. T. (2008) Production, oxygen respiration rates, and sinking velocity of copepod fecal pellets: direct measurements of ballasting by opal and calcite. *Limnol. Oceanogr.* **53**, 469–476.
- Rae J., Foster G., Schmidt D. and Elliot T. (2011) Boron isotopes and B/Ca in benthic foraminifera: proxies for the deep ocean carbonate system. *Earth Planet. Sci. Lett.* **302**, 403–413.
- Ragueneau O. and Tréguer P. (1994) Determination of biogenic silica in coastal waters: applicability and limits of the alkaline digestion method. *Mar. Chem.* **45**, 43–51.
- Ragueneau O., Savoye N., Del Amo Y., Cotten J., Tardiveau B. and Leynaert A. (2005) A new method for the measurement of biogenic silica in suspended matter of coastal waters: using Si/Al ratios to correct for the mineral interference. *Cont. Shelf Res.* **25**, 697–710.
- Ragueneau O., Tréguer P., Leynaert A., Anderson R. F., Brzezinski M. A., DeMaster D. J., Dugdale R. C., Dymond J., Fischer G., François R., Heinze C., Maier-Reimer E., Martin-Jézéquel V., Nelson D. M. and Quéguener B. (2000) A review of the Si cycle in the modern ocean: recent progress and missing gaps in the application of biogenic opal as a paleoproductivity proxy. *Global Planet. Change* **26**, 317–365.
- Riebesell U., Zondervan I., Rost B., Tortell P. D., Zeebe R. E. and Morel F. M. M. (2000) Reduced calcification of marine plankton in response to increased atmospheric CO<sub>2</sub>. *Nature* **407**, 364–367.
- Rollion-Bard C. and Erez J. (2010) Intra-shell boron isotope ratios in the symbiont-bearing benthic foraminiferan *Amphistegina lobifera*: implications for delta d<sup>11</sup>B vital effects and paleo-pH reconstructions. *Geochim. Cosmoch. Acta* **74**, 1530–1536.
- Rost B., Richter K. U., Riebesell U. and Hansen P. J. (2006) Inorganic carbon acquisition in red tide dinoflagellates. *Plant, Cell Environ.* **29**, 810–822.
- Rost B., Kranz S. A., Richter K. U. and Tortell P. D. (2007) Isotope disequilibrium and mass spectrometric studies of inorganic carbon acquisition by phytoplankton. *Limnol. Oceanogr. Methods* **5**, 328–337.
- Sanyal A., Nugent M., Reeder R. J. and Bijma J. (2000) Seawater pH control on the boron isotopic composition of calcite: evidence from inorganic calcite precipitation experiments. *Geochim. Cosmochim. Acta* **64**, 1551–1555.
- Schröder H. C., Perovic-Ottstadt S., Grebenjuk V. A., Engel S., Müller I. M. and Müller W. E. G. (2005) Biosilica formation in spicules of the sponge *Suberites domuncula*: synchronous expression of a gene cluster. *Genomics* **85**, 666–678.
- Seki O., Foster G. L., Schmidt D. N., Mackensen A., Kawamura K. and Pancost R. D. (2010) Alkenone and boron-based Pliocene pCO<sub>2</sub> records. *Earth Planet. Sci. Lett* **292**, 201–211.

- Stoll H., Langer G., Shimizu N. and Kanamaru K. (2012) B/Ca in coccoliths and relationship to calcification vesicle pH and dissolved inorganic carbon concentrations. *Geochim. Cosmochim. Acta* **80**, 143–157.
- Tachibana M., Allen A. E., Kikutani S., Endo Y., Bowler C. and Matsuda Y. (2011) Localization of putative carbonic anhydrases in two marine diatoms, *Phaeodactylum tricornerutum* and *Thalassiosira pseudonana*. *Photosynth. Res.* **109**, 205–221.
- Takano J., Noguchi K., Yasumori M., Kobayashi M., Gajdos Z., Miwa K., Hayashi H., Yoneyama T. and Fujiwara T. (2002) *Arabidopsis* boron transporter for xylem loading. *Nature* **420**, 337–340.
- Tanaka M. and Fujiwara T. (2008) Physiological roles and transport mechanisms of boron: perspectives from plants. *Pflug. Arch. Eur. J. Physiol.* **456**, 671–677.
- Taylor N. J. (1985) Silica incorporation in the diatom *Coscinodiscus granii* as affected by light intensity. *Brit. Phycol. J.* **20**, 365–374.
- Tepel M., Nesbit O., Tokmak F. and Zidek W. (1998) Sodium-dependent  $\text{Cl}^-/\text{HCO}_3^-$  exchange in patients with chronic renal failure: correlation with renal function. *Kidney Int.* **53**, 432–438.
- Tortell P. D. (2000) Evolutionary and ecological perspectives on carbon acquisition in phytoplankton. *Limnol. Oceanogr.* **45**, 744–750.
- Tortell P. D. and Morel F. M. M. (2002) Sources of inorganic carbon for phytoplankton in the eastern Subtropical and Equatorial Pacific Ocean. *Limnol. Oceanogr.* **47**, 1012–1022.
- Tortell P. D., Martin C. L. and Corkum M. E. (2006) Inorganic carbon uptake and intracellular assimilation by subarctic Pacific phytoplankton assemblages. *Limnol. Oceanogr.* **51**, 2102–2110.
- Tortell P. D., Reinfelder J. R. and Morel F. M. M. (1997) Active uptake of bicarbonate by diatoms. *Nature* **390**, 243–244.
- Trimborn S., Wolf-Gladrow D., Richter K. U. and Rost B. (2009) The effect of  $\text{pCO}_2$  on carbon acquisition and intracellular assimilation in four marine diatoms. *J. Exp. Mar. Biol. Ecol.* **376**, 26–36.
- Vrieling E. G., Gieskes W. W. C. and Beelen T. P. M. (1999) Silicon deposition in diatoms: control by the pH inside the silicon deposition vesicle. *J. Phycol.* **35**, 548–559.
- Wang Z., Hattendorf B. and Günther D. (2006) Analyte response in laser ablation inductively coupled plasma mass spectrometry. *J. Am. Soc. Mass Spectrom.* **17**, 641–651.

Associate editor: Jack J. Middelburg